Combusted-diesel additives containing CeO 2 nanomaterials shape methanogenic pathways during sludge digestion and enhance biogas production

Mélanie Auffan, Abdoul Karim Kabore, Anais Cuny, Oulfat Amin Ali, Mohammed Barakat, Bernard Angeletti, Olivier Proux, Jean-Yves Bottero, Nicolas Roche, Catherine Santaella

Combusted-diesel additives containing CeO_2 nanomaterials shape methanogenic pathways during sludge digestion and enhance biogas production

Auffan Mélanie[a,b], Kabore Abdoul Karim[a], Cuny Anais[a,c], Amin Ali Oulfat[c], Barakat Mohamed[c], Angeletti Bernard[a], Proux Olivier[d], Bottero Jean-Yves[a,b], Roche Nicolas[a,e], Santaella Catherine[c]

a. *CEREGE, CNRS, Aix Marseille Univ, IRD, INRAE, Aix-en-Provence, France*
b. *Civil and Environmental Engineering, Duke University, Durham, NC 27708, USA*
c. *Aix Marseille Univ, CEA, CNRS, BIAM, LEMIRE, Saint-Paul-Lez-Durance, France*
d. *OSUG, UAR 832 CNRS - Univ. Grenoble Alpes, IRSTEA, INRAe, Météo-France, Grenoble, France*
e. *International Water Research Institute (IWRI), Mohammed VI Polytechnic University, Ben Guerir 43150, Morocco*

This study addressed the impact of nanomaterials on anaerobic digestion and biogas production (methanogenesis pathways) when contaminanting aerobic sludge generated during wastewater treatment. Our experimental system was based on bioreactor operational parameters aligned with the operating conditions used in wastewater treatment plants (WWTP), a contamination scenario considering the treatment of nano-enabled products at the last stages of their life cycle, and nanomaterial concentrations close to those predicted in WWTP. The physico-chemical, microbiological and chemical engineering proxies studied all concluded that combusted nanoCeO_2-enabled fuel additives transiently increased EPS production and specific hydrolytic enzymatic activities without altering the aerobic sludge microbial community structure nor the C, P, N removal capacity (spiked concentrations of 130 µg.L^{-1} during aerobic sludge production). However, the presence in the aerobic sludge biosolids of 99.9 % of the total CeO_2 injected (without any change in speciation) altered the production, structure, and activity of the anaerobic sludge during digestion (impacting the EPS, ATP, lipase and **α**–glucosidase activities). Interestingly, these modifications of the anaerobic sludge activity shaped the methanogenesis pathways from acetoclastic to hydrogenotrophic and enhanced the biogas production with a significant increase in generated H_2. In the context of developing a sustainable energy supply, we observed a continuous improvement of the biogas production in the contaminated bioreactor, which could increase the energy recovery potential of WWTPs.

Introduction

In the context of the energy transition, waste-to-energy plants are of paramount importance. They significantly reduce the volume of waste entering landfills and provide alternatives to fossil fuels. Anaerobic digestion (AD) of sewage sludge has attracted considerable attention to convert waste into biogas (e.g. CH_4, CO_2 and H_2) and understanding the mechanisms that control biogas yield during wastewater sludge digestion is crucial. In the past few years, emerging pollutants (e.g. pharmaceuticals, pesticides, nanomaterials) found in surface water, groundwater, and drinking water have reached wastewaters at ng.L^{-1} or µg.L^{-1} concentrations [1,2]. Since these pollutants can induce harmful effects on living organisms, their ability to be effectively treated in urban and industrial wastewater treatment plants (WWTP) and to simultaneously impact sludge valorization pathways requires investigation.

Among emerging pollutants, WWTP are known to be primary collectors for nanomaterials (NMs) [3,4] all along NMs' lifecycle, i.e. from the production of pristine nanoparticles and the use of nano-enabled products to their end-of-life [8,9]. NMs have been found to be efficiently treated in WWTP with 70 to 99% removal, leading to concentrations in waste activated sludge and anaerobic sludge between 0.01 to 0.4 µg.L^{-1} for Cd, Au, Al, Ag and Co-based NMs and from 4.6 to 39.9 µg.L^{-1} for Ni, Mn, Cu, Zn, Mg, Ce, Fe and Ti-based NMs [1,2]. The mechanisms of NM removal from wastewater greatly depend on NM chemistry, size, crystallinity, coating and concentration. For instance, TiO_2 and CeO_2 NM removal is mainly driven by hetero-aggregation and sorption on biosolids [10,11], while Ag NM removal is driven by oxidative dissolution/reprecipitation into AgCl and Ag_2S due to interactions with cysteine or humic acids [12,13]. Regarding biogas production, the presence of NMs during AD has been shown to affect the hydrolysis of organic matter and methanogenesis *via* the release of metal ions (Ag, Zn and Cu) [14–16], but also *via* physical penetration, membrane shrinking, and oxidizing effects on the outer membranes of micro-organisms [17–19]. In contrast, low solubility NMs (e.g. TiO_2) have not shown any adverse effects due their chemical stability and the protective role of extracellular polymeric substances (EPS) [16].

For some NMs (e.g. CeO_2), the published results are contradictory depending on the contaminants used. García et al. (2012) have shown great inhibition of biogas production after 50 days of AD in the presence of pristine CeO_2 NMs (640 mg L^{-1}) [17]. At these concentrations, the anaerobic bacterial populations were drastically inhibited [17]. On the other hand, Ünsar et al. (2016) measured only 5.5 % inhibition of methane production following exposure to 5680 mg.L^{-1} pristine CeO_2 NMs [20]. It is noteworthy that the bioreactor operational settings in these studies poorly represented the conditions

that CeO_2 NMs would encounter during AD of sludg in the following ways: *(i)* direct loading of NMs in digestors, *(ii)* using pristine NMs (first stage of the NMs lifecycle) instead of the more relevant aged nano-enabled product (end-of-life stage), *(iii)* synthetic wastewater as feeding source instead of real wastewater, *(iv)* testing concentrations of NMs orders of magnitude higher than the environmental predictions, and *(v)* operating conditions far from the ones used in WWTP (*e.g.* sludge residence time). A few studies have developed more relevant exposure scenarios by feeding the AD with activated sludge (AS) previously spiked with a mixture of pristine NMs [4,21] or by spiking aged nano-enabled products directly in AD. [22,23] This last point is of particular importance since changes in redox state, aggregation/agglomeration state, surface properties, and matrix/nanoparticle interactions during aging could alter the biosolids valorization as compared to pristine NMs [21]. For instance, CeO_2 NMs have been used as a fuel-borne catalyst in diesel engines for about 20 years [24]. Several studies have focused on the release of cerium through diesel exhausts especially in urban areas i.e. the physico-chemical transformations of the NMs after combustion and the predicted Ce concentrations in soil, water, air, and WWTP through waste streams [25–31]. During combustion, however, the structural and physico-chemical properties of the combusted CeO_2 NMs-based diesel additives drastically change compared to pristine NMs: *(i)* the size of the CeO_2 particles increases, *(ii)* they became more crystallized without detectable Ce(III) in their structure, and *(iii)* the organic compounds of the additive fully degrade [29,32,33]. Moreover, regardless of the aging conditions (salinity, light, pH), the dissolution kinetics of the combusted CeO_2 particles were slower than pristine CeO_2 NMs [33]. Interestingly, some studies have focused on the biological impacts of these combusted (i.e. aged) CeO_2 NMs [34,35] and have observed different effects as compared to pristine CeO_2 NMs.

Herein, we combined expertise in chemical engineering, microbiology and physical chemistry to assess the impacts of combusted CeO_2 NM-based diesel additives (i.e. the latest stage of their lifecycle) on digestor operation and biogas production in WWTPs. More specifically, we addressed *(i)* how aged CeO_2 NMs released from combustion alter the production, structure, and activity of anaerobic sludge, and *(ii)* how this impacts the mechanisms of biogas production as well as their quantity. In this research, we addressed limitations observed in past studies by: loading NMs into AS which was fed to AD, using combusted CeO_2 NMs and real wastewater, testing relevant CeO_2 concentrations in the upper ranges of those predicted in influents and biosolids, and using solid retention times relevant to WWTPs.

Materials and methods

Influent wastewater and sludges collection

Wastewater and sludges were collected from a local urban and industrial WWTP (Aix-en-Provence, France 160 000 inh. eq.). Wastewater was sampled after primary treatment (screening, de-gritting, de-oiling). The total chemical oxygen demand (COD) of the influent was 1.008 mg O_2.L^{-1} on average; with 106.1 mg.L^{-1} ammonium - nitrogen (NH_4^+ - N), 0.7 mg.L^{-1} nitrate - nitrogen (NO_3^- - N). The wastewater sampled was divided in aliquots of 300 mL that were stored at –25 °C. The activated sludge was sampled in the sludge recycle line of the aeration basin. The concentration of the initial total suspended solids (TSS) was ~3 g.L^{-1} in the mixed liquor. This sludge was concentrated up to 7 g.L^{-1} after a few hours (3 to 4h) of settling. The inoculum for the anaerobic digestion was sampled from the mesophilic digester. The anaerobic digester presented a mean TSS of 40 g.L^{-1} a volatile suspended solid (VSS) of 80%.

Activated sludge (AS) production

Two individual gas-tight glass sequential batch reactors (control and spiked with combusted CeO_2 NMs) were filled with 5 L of an initial mixed liquor with TSS of 7 g.L^{-1} to produce activated sludge (AS) for the following anaerobic digestion (AD). Everyday 300 mL of mixed liquor were withdrawn from the reactors and 300 mL of pretreated wastewater was thawed and added to keep a sludge residence time (SRT) of 16.7 days. To compensate for the C/N ratio of the influent and to promote the sludge production for future use in the AD, 3 g of glucose were added to the 300 mL of pretreated wastewater daily.

The pH in both control and contaminated bioreactors were kept between 7.4 and 7.5. The temperature was maintained at 21 °C. The reactors were continuously stirred at 200 rpm for 40 days, and successively aerated at 1/3 vvm for 23 hours and non-aerated for 1 hour. At the end, the AS from control and contaminated reactors were divided in 20 aliquots of 250 mL stored at -25 °C for the next AD step. The treatment operating parameters are shown in supporting information (see SI, **Erreur ! Source du renvoi introuvable.**).

Combusted Envirox™

We contaminated the real WWTP influent with an aged nano-enabled fuel additive, called Envirox™ supplied by Energetics Europe Ltd. Envirox™ has been used to reduce particulate emissions in diesel vehicles, based on the catalytic properties of CeO_2 [36]. To mimic the combustion in a diesel engine, Envirox™ was burned in a furnace at 850°C [25,28–31], and the CeO_2 byproducts of the combustion (comb-CeO_2 NMs) were injected in lab-scale bioreactors. The

protocol used to generate the comb-CeO_2 NMs and their thorough physico-chemical characterization was published in ref. [33] (see **Erreur ! Source du renvoi introuvable.**).
Briefly, the diesel additive was ultracentrifuged (396 750g, 20 °C, 1 h), freeze-dried, and combusted (100 mg, 20 min, 850°C). After combustion, the mean size of the CeO_2 nanoparticles increased from 7.6 ± 1.2 nm (before combustion) to 19 ± 10 nm (after combustion). The coherent diameters also increased from 5.5 ± 0.5 nm (before) to 21.0 ± 2.3 nm (comb-CeO_2 NMs) with a constant inter-reticular distance d_{hkl} of 3.1 Å corresponding to cerianite. The complete degradation of the organic matrix initially surrounding the CeO_2 particles was observed for the comb-CeO_2 NMs by infra-red spectroscopy [33].
A stock suspension of the comb-CeO_2 NMs was prepared at 500 mg $CeO_2.L^{-1}$ and used to contaminate the AS. Aliquots of 1.3 mL or 2.6 mL (i.e. 130 µg.L^{-1} or 260 µg.L^{-1} as spiked concentrations) were used to feed the AS three times a week during 40 days to reach a final concentration of 2.8 mg $CeO_2.L^{-1}$. The contaminated AS were then anaerobically digested for 29 days with a final concentration of 2.2 mg $CeO_2.L^{-1}$.

Anaerobic digestion (AD) of the activated sludge

In order to maintain a constant sludge residence time of 20 days *(i)* the inoculum size sampled in the AD of the WWTP was 5L and, *(ii)* 250 mL of AS was removed as sample and replaced by 250 mL of AS (from control and comb-CeO_2 NMs aerobic reactors) on a daily basis. Feeding the digestors with contaminated AS simulated a real NM contamination scenario in a WWTP. As in Aix-en-Provence's WWTP, the AD temperature was set at 37°C with cold and hot water circulation in the reactor jacket. The pH was set at 7.4 by daily dosing NaOH (4 M). In the AD, the higher content of TSS made sludge viscous. To ensure homogeneous mixing of contaminated sludge in the digestors, the culture broth was stirred at 500 rpm. Biogas was collected at the top of the digestion tank, compressed, and released through a series of immersed devices. Gas flowrates were continuously measured by a MilliGas counter (RITTER MGC-1). The experiment was performed for 29 days, and the process parameters monitored are given in supporting information (see SI, Figure S 5).

Nitrogen and phosphorus

Nitrogen removal efficiency was estimated by measuring daily nitrate and ammonium content in bioreactors using an AN-ISE probe (HACH Lange, France) equipped with ion-selective electrodes, specific for wastewater. The phosphorus removal efficiency was estimated by measuring total phosphorus content, following the APHA standard method [26].

Enzymatic activities, active biomass and EPS contents

α-glucosidase activity was measured with p-nitrophenyl **α**-D-glucopyranoside degradation and protease activity with azocasein degradation [38]. Lipase activity was measured using a modified protocol of Kim et al. [39]. The active biomass content being directly related to ATP concentration was measured using BactTiter-glo® kit (Promega corporation). The extraction of EPS in AS culture was performed using a modified version of Dubois's method [40].

Cerium distribution and transformation

The distribution of Ce between the solid and liquid phase of the mixed liquor were measured by ICP-MS (PerkinElmer, NexIon 300X). Every week, 50 mL from both bioreactors were centrifuged at 4000g for 15 min. 10 mL of the liquid phase were acidified with 10 µL HNO_3 15 N. 5 mL of the liquid phase were ultrafiltered (Amicon Ultra-4, 3 kDa) to measure the Ce dissolved fraction and acidified with 10 µL HNO_3 15 N. The solid phase from centrifugation was freeze-dried, pressed into 5 mm pellets, and analyzed by HERFD XANES (High Energy Resolution Fluorescence Detection of X-ray Absorption Near Edge Structure) at the cerium L_3–edge on the FAME-UHD beamline (BM16) at the ESRF-Grenoble synchrotron light source (France). Samples were analyzed in fluorescence mode using a crystal analyzer spectrometer equipped with Si(331) crystals (radius of curvature of 1m) [41]. The incident photons' energy was calibrated using a micron-sized CeO_2 reference compound (first maximum of the spectrum first derivative set at 5725.6 eV). Frozen pellets were analyzed using a liquid helium cryostat, in order maximally limit radiation damage during acquisition. The resulting spectrum for each sample was the sum of at least three scans. Data reduction was performed using an IFEFFIT software package [42]. Comb-CeO_2 NMs, micron-sized CeO_2 particles, and Ce(III)-phosphate, were used as Ce(IV) and Ce(III) reference compounds.

Microbial community

Total DNA was extracted in triplicate from each AD and at each time point, from 3 different samples, using FastDNA SPIN Kits for Soil and FastPrep-24 Instrument (MP Biomedicals; Illkirch, France), according to the manufacturer's instructions. The variable regions V4 of bacterial 16S rRNA gene were amplified with the specific primers 515F-Y (5'-GTGYCAGCMGCCGCGGTAA) [43] and 806RB (5'- GGACTACNVGGGTWTCTAAT) [44]. The amplicons were checked on 1% agarose gel. DNA concentration and purity were checked using a NanoVue (NanoVue-NV-GE, Healthcare Limited;

Uk) and a Qubit fluorometer (ThermoFisher Scientific, FR). Polymerase chain reaction (PCR) reactions were carried out using HotStarTaq Plus Master Mix Kit (Qiagen; FR). PCR products were purified using ProNex® Size-Selective DNA Purification System (Promega, FR). The preparation of the library, indexation and sequencing were performed at the ICM Plateforme/Service de Génotypage Séquençage (Hôpital Pitié-Salpétrière, Paris). The amplicons (20 ng) were used for the DNA library preparation using Nextera XT DNA Library Prep Kit for Illumina. After quality control (Tape Station, Aglient) and quantification (QuantiFluor® dsDNA System, Promega), amplicon sequencing was performed on a MiSeq Illumina instrument (Illumina, Inc., San Diego, USA) to generate 25 M, 300 bp paired-end reads.
rRNA amplicon forward sequences were analyzed using QIIME2 (qiime2:2019.10.0) [45]. Sequences were demultiplexed, truncated at 260 nucleotides based on sequence quality profile (>25), denoised and chimeras were removed using DADA2 [46]. Sequences were aligned using MAFFT [47] and were used to construct a phylogeny using FastTree [48]. Taxonomy was assigned using a Naïve Bayes classifier trained on the GreenGenes database (version 13_8). After rarefaction, 1342 features were generated from 73,320 reads from 36 samples. Beta diversity principal coordinates analysis (PCoA, weighted UniFrac distances dissimilarity) was generated using QIIME2 and visualized using XLSTA. Bar plots were generated in Microbiome Analyst (https://www.microbiomeanalyst.ca/). Feature volatility anaylsis was performed with the q2-longidinal plugin for QIIME2 [49].

Statistical analysis

Statistical analyses (Kruskall-Wallis, ANOVA, PERMANOVA, PERMDIST, were performed in R (http://www.R-project.org), or in XSTAT (2019.3.2). $P < 0.05$ was considered to be statistically significant.

Results and discussion

Unaltered bio-physico-chemical properties of the activated sludge contaminated with combusted CeO_2 NMs

To characterize the AS used for AD, we studied the Ce distribution and speciation in liquid and biosolid phases. After 40 days, only a negligible concentration of Ce was measured in the effluent with 99.9 % of the initial mass of Ce found in the biosolids (Figure 1). The near-neutral net surface charge of the comb-CeO_2 NMs at the pH and ionic strength of the AS favors aggregation, interactions with the sludge flocs, and efficient removal by settling, which has been previously demonstrated [1,2,9,50–53]. The speciation of the Ce in the settled flocs was determined by HERFD-XANES spectra at the Ce L_3-edge (Figure 1). HERFD-XANES signature of Ce(III) is characterized by one pre-edge and one main edge at 5718 eV and 5726 eV, respectively, while Ce(IV) has one pre-edge at 5720 eV and three main features at 5727, 5730, and 5738 eV. Pre-edge analysis in the HERFD-XANES spectra of biosolids showed that no chemical reduction of Ce(IV) into Ce(III) occurred during AS production. Differences in the edge features between comb-CeO_2 and Ce in the AS at Day 40, especially the well-defined peak at 5727 eV, could be due to size effects [54]. In contrast, Barton et al. (2014) observed 44±4 % and ~31±3 % chemical reduction of Ce(IV) in AS contaminated with pristine and citrated-coated CeO_2 NMs (with average diameters of 3–4 nm), respectively after 5 weeks. They attributed this chemical reduction to interactions with bacteria [53]. Herein, CeO_2 particles after combustion had a larger size, a high polydispersity (19 ± 10 nm), and a higher crystallinity [33] than their work, which slowed down the (bio)transformation kinetics in AS despite the microbial activity. CeO_2 NMs are considered transient due to their partial (bio)conversion to Ce(III), in WWTP [49], sludge incineration [55], soils [56], and plants [57]. However, our results show that combustion makes Ce(IV) nanoparticles more persistent than expected, probably because of their higher post-combustion crystalline stability and subsequent slower transformation kinetics.
PCA was used to examine the underlying structure of the whole data set generated during the AS production, termed the individual, as well as the interrelations among several variables within the data set (*e.g.* EPS, ATP, N and P concentrations, enzymatic activities) during the production of pristine- and comb-CeO_2 NM-contaminated-AS [58]. The two first principal components F1 and F2 accounted for 56.51% and 19.72% of the variability, respectively. PCA shows that none of the measured variables were significantly correlated to the concentration of comb-CeO_2 NMs in the bioreactor ($p \geq 0.05$) (Figure 2). The overall performance in terms of COD, phosphorus, and nitrogen removal was not significantly different between control and contaminated reactors. The phosphorus concentration gradually decreased from 6 to 2 $mg.L^{-1}$, and full nitrification with more than 95% nitrogen removal was obtained after 40 days (**Erreur ! Source du renvoi introuvable.**). No changes in the AS microbial community structure were observed between the control and contaminated AS (**Erreur ! Source du renvoi introuvable.**). Comparing control and contaminated AS, ANOVA tests highlighted transient impacts (p-value<0.05) of comb-CeO_2 NM contamination on enzyme activities and tightly bound EPS (TB-EPS) concentrations (**Erreur ! Source du renvoi introuvable.**). However, over their lifetimes the two reactors were observed to behave similarly. Using up to 50 $mg.L^{-1}$ of pristine CeO_2 NPs in sequential batch reactors, You et al. (2015) also observed an increase of 28 % for the loosely bound EPS (LB-EPS) and 39 % for the TB-EPS production associated with a decrease in the flocculating capacity of the EPS and a shift to different EPS functional groups (-OH, -NH_2) [59]. These previously observed responses of the AS in conditions far from real operating conditions were attributed

to a defense mechanism preventing the contact between metallic NPs and bacteria inside flocs [18,60–62], which we did not observe under realistic AS conditions.

Consequently, at the realistic concentrations used in this study (2.8 mg.L^{-1}) and at the late-stage of the lifecycle , all the physico-chemical and biological proxies measured concluded that comb-CeO_2 NMs transiently increased the EPS production and some hydrolytic enzymatic activities in the produced AS, but did not affect the microbial community structure nor the removal capacity (COD, phosphorus, nitrogen). After 40 days, the biosolids produced to feed the AD contained 99.9 % of the total Ce with a speciation similar to the one initially injected.

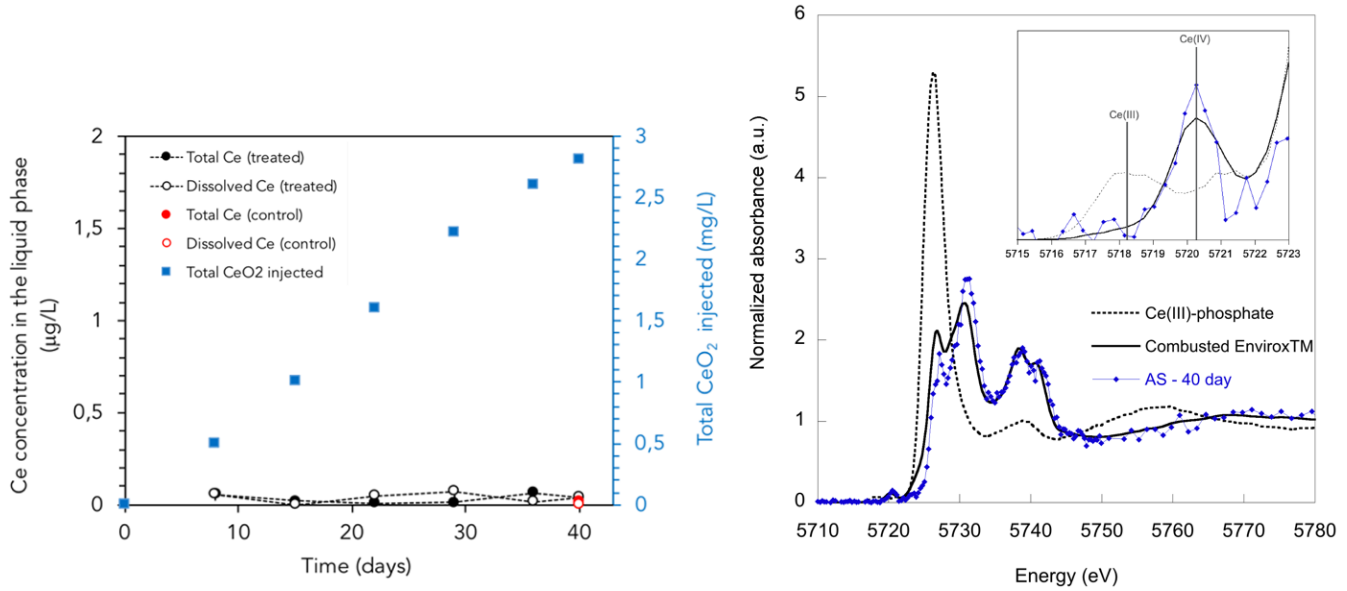

Figure 1. Distribution and speciation of Ce during aerobic sludge production. (Left) Total and dissolved (<3 kDa) Ce concentrations remaining in the liquid phase after separation by centrifugation of the aerobic sludge (Black symbols). Blue squares represent the total concentration of comb-CeO_2 NMs (in mg CeO_2.L^{-1}) injected in the bioreactors over 40 days. Red circles represent the Ce concentration in the liquid phase of control bioreactors at the end of the experiment. Values are means of three repetitions ± standard deviation. (Right) Experimental HERFD-XANES spectra at the Ce L_3-edge in the aerobic sludge dosed with combusted CeO_2 NPs. Experimental XANES spectrum is compared to Ce (III)-phosphate and a comb-CeO_2 NM reference compound (Envirox™). The inset corresponds to the pre-edge area.

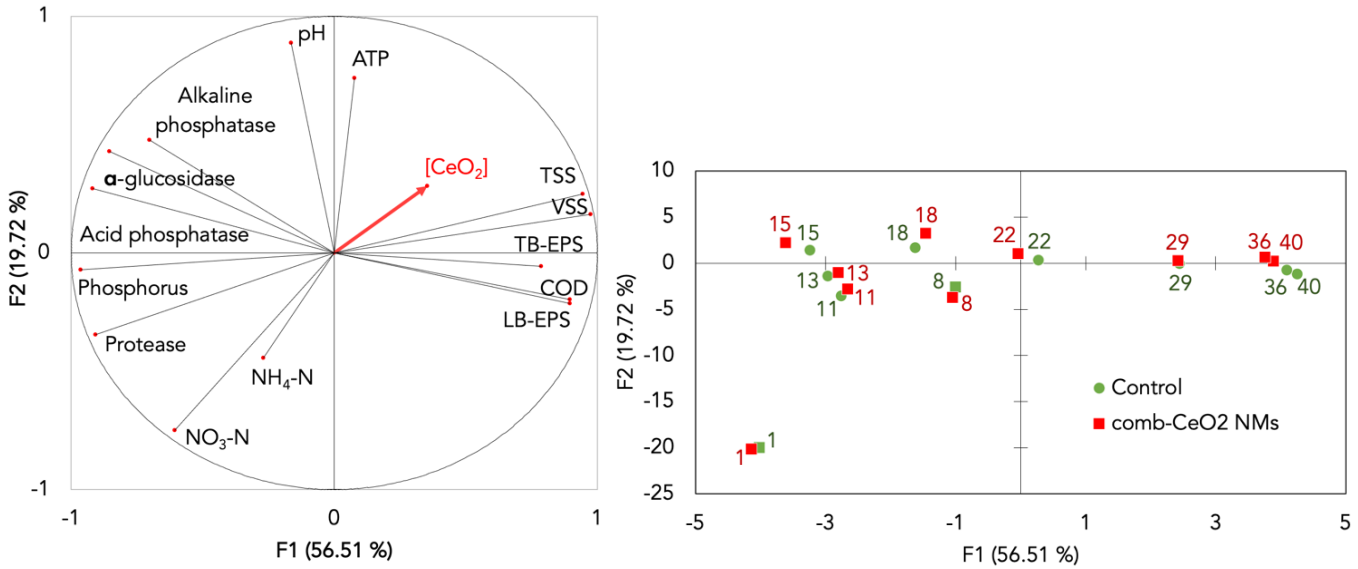

Figure 2. Principal component analysis of the variables measured during control and comb-CeO_2 NM contaminated-aerobic sludge production. The first two principal components F1 and F2 explained 56.51% and 19.72% of the variability, respectively. (Left) The correlation circle plot of all variables highlights the relationships between the response variables of the first two components. None of the variables measured were significantly correlated to the comb-CeO2 NMs in the bioreactor ($p \geq 0.05$) (red). (Right) Observation plot. Each red or green symbol corresponds to one observation i.e. the complete set of data measured on a reactor on a given day and for a given condition. No significant differences were observed between control and contaminated bioreactors at any given time ($p \geq 0.05$).

Altered bio-physico-chemical properties of anaerobic sludge feed with contaminated aerobic sludge

As previously observed in AS and in agreement with the literature [2], more than 99.9 % of the Ce injected during AD (2.2 mg $CeO_2.L^{-1}$) remained in the biosolid phase (**Erreur ! Source du renvoi introuvable.**). After 29 days of AD, the total concentration of Ce measured in the liquid phase was ~0.5 µg.L^{-1} (*i.e.* similar to the Ce concentrations in controls) and the dissolved Ce concentrations were below the detection limit. Despite the Eh (~ – 438 mV), pH (~7.4), and the presence of complexing molecules, the Ce oxidation state of the comb-CeO_2 NMs remained unchanged (**Erreur ! Source du renvoi introuvable.**). The HERFD-XANES in **Erreur ! Source du renvoi introuvable.**, presented differences in the intensity (but similar position in energy) of the main absorption edges corresponding to Ce(IV) after AD. This could be attributed to changes in the short-range order of the CeO_2 structure in the form of atomic rearrangements at the surface following adsorption on micro-organisms or complexation with EPS [62,63].

PCA (Figure 3) was used to examine the underlying structure of the individuals and the interrelations among the variables (*e.g.* EPS, ATP, N and P concentrations, enzymatic activities). In Figure 3, as previously, the individual represents the whole data set generated during AD. The two first principal components F1 and F2 accounted for 50.49% and 19.81% of the variability, respectively. PCA shows that neither TSS nor VSS was significantly correlated to the concentration of comb-CeO_2 NMs in the bioreactor (p>0.05). The rheological response was also measured and no statistical difference was observed between the bioreactors (p>0.05) in terms of flow index, yields stress, and consistency index (data not shown). However, comparing control and contaminated AD, ANOVA tests highlighted impacts (p<0.05) of the contamination on TB-EPS (R=0.76) and LB-EPS (R=-0.64) from day 0 to days 27 and 29 respectively (Figure 3 and Figure 4). Effects of comb-CeO_2 NMs were also observed on hydrolytic enzymatic activities; with lipase (R=0.62) and **α**–glucosidase (R=0.60) activities significantly increasing after 22 days of exposure (CeO_2 concentrations > 1.9 mg.L^{-1}) (Figure 4). These increases were correlated with an increase of the biomass activity represented as the amount of ATP (R=0.62) produced (**Erreur ! Source du renvoi introuvable.**).

Mu et al. (2011) studied the effects of ZnO NMs (1 500 mg L^{-1}) on the short chain fatty acids during the acidification step [64]. At such high concentrations, the activities of protease, acetate kinase and coenzyme F_{420} were respectively inhibited by 25 %, 23 % and 41 % after 18 days of digestion and these effects were attributed to ion release. Interestingly, Chen et al. (2014) compared direct and indirect (during aerobic sludge production) spiking modes of Cu NMs in sludge digestion and showed that only direct spiking of Cu NMs resulted in a 50% decrease of protease and 64% decrease of glucosidase activities, and maximal VFA production [14]. More than the dose (2.2 mg.L^{-1}), the experimental strategy chosen herein could be responsible for the observed change in sludge activity *i.e.* (i) indirect spiking during the AS production followed by the subsequent AD of the sludge and (ii) contamination with comb-CeO_2 NMs that are chemically more stable (Figure 1, **Erreur ! Source du renvoi introuvable.**) than pristine NMs.

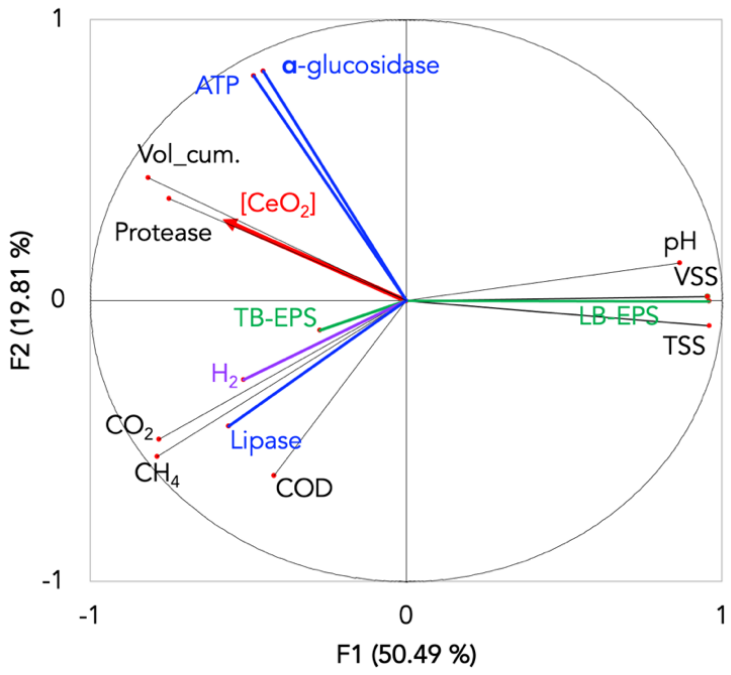

Figure 3. Principal component analysis of the variables measured during the AD production fed or not with AS contaminated comb-CeO_2 NMs. The correlation circle plots all the variables against the two first principal components F1 and F2, which account for 50.49% and 19.81% of the variability, respectively.

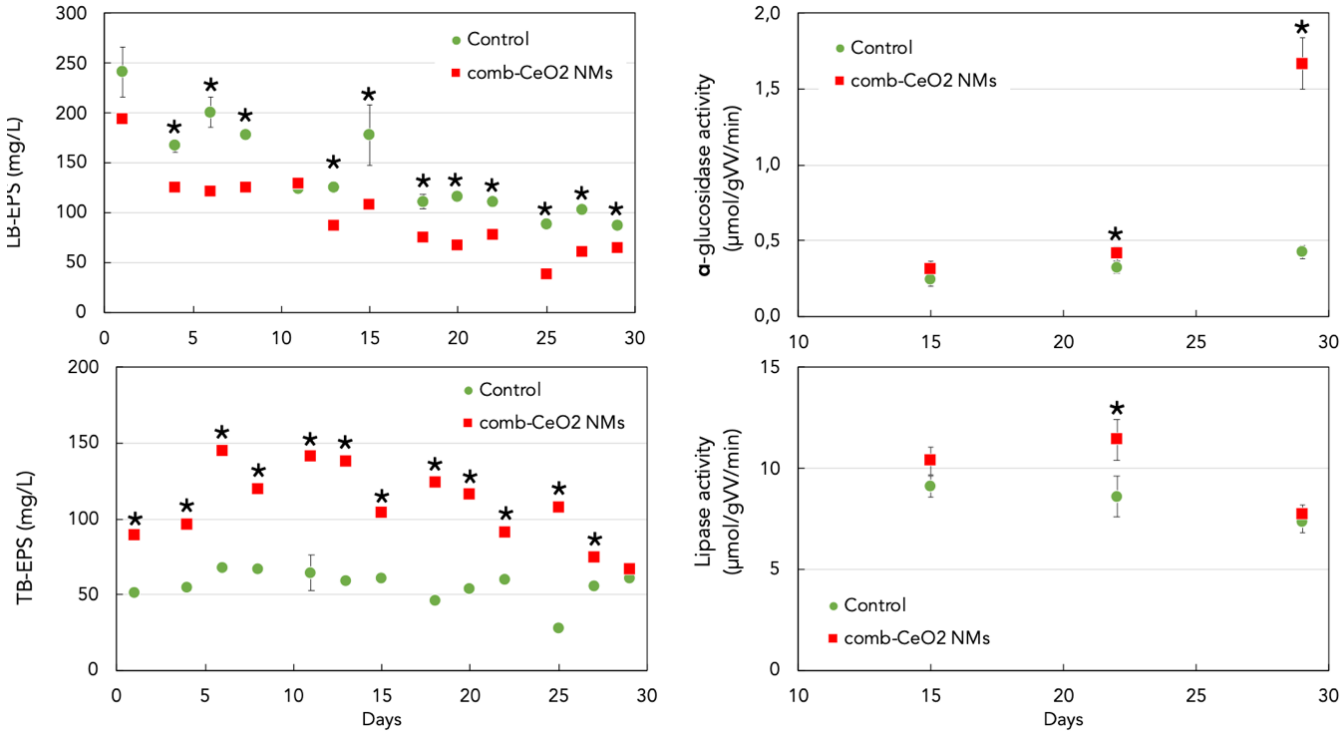

Figure 4. Comparison of tightly bound (TB-EPS) and loosely bound-EPS (LB-EPS) as well as enzymatic activities (α-glucosidase and lipase) in AD in the presence and absence of comb-CeO_2 NMs. * Represents data that are statistically significant (p<0.05) at a given time point. Values are average ± standard deviation.

Combusted CeO_2 NMs alter biogas production and methanogenic pathway during sludge digestion

Biogas production in the presence of comb-CeO_2 NMs was monitored over time. Figure 5 showed that daily biogas production was always higher in the contaminated AD (Figure 5) with a constant production rate from day 18 to 28 in both reactors. During that period, the biogas volume production was 18% higher in the contaminated AD (~1.85 L/day) than in the control (~0.57 L/day) with similar biomass concentrations in the two reactors (5.7 and 5.9 g $VSS.L^{-1}$ respectively) at the end of the experiments (**Erreur ! Source du renvoi introuvable.**).

PCA (Figure 3) corroborates this result showing that the concentration of comb-CeO_2 NMs is significantly correlated to the amount of H_2 (p<0.05; R=0.57) but not to the amounts of CH_4 and CO_2 (p>0.05). Methane production during AD of sludge includes different steps, namely, hydrolysis, acidogenesis, acetogenesis and methanogenesis [65]. While the acetogenesis step is carried out by *bacteria*, the methanogenesis step is driven by a specialized microbial group of *archaea*. These *archaea* are known to be highly sensitive to variations in temperature, pH, C/N ratio, as well as sludge properties [66]. To understand the observed changes in biogas production, microbial consortia of *archaea* and *bacteria* were studied in terms of community structure and composition (Figure 6 and **Erreur ! Source du renvoi introuvable.**). The first two axes of the Principal Coordinate Analysis (PCoA) based on weighted UniFrac distances (phylogeny and abundance of Operational Taxonomic Units, OTUs) explained 77.6% of the community dissimilarity (Figure 6). A weighted-unifrac-pairwise-distances-time revealed that the bacterial community structure between the control and contaminated AD started to differ at Day 11. Based on a PERMANOVA from Day 18 to 29, the time variable explained 57.1% (p<0.05) of the variability, and the treatment accounted for 21.7% (p<0.05).

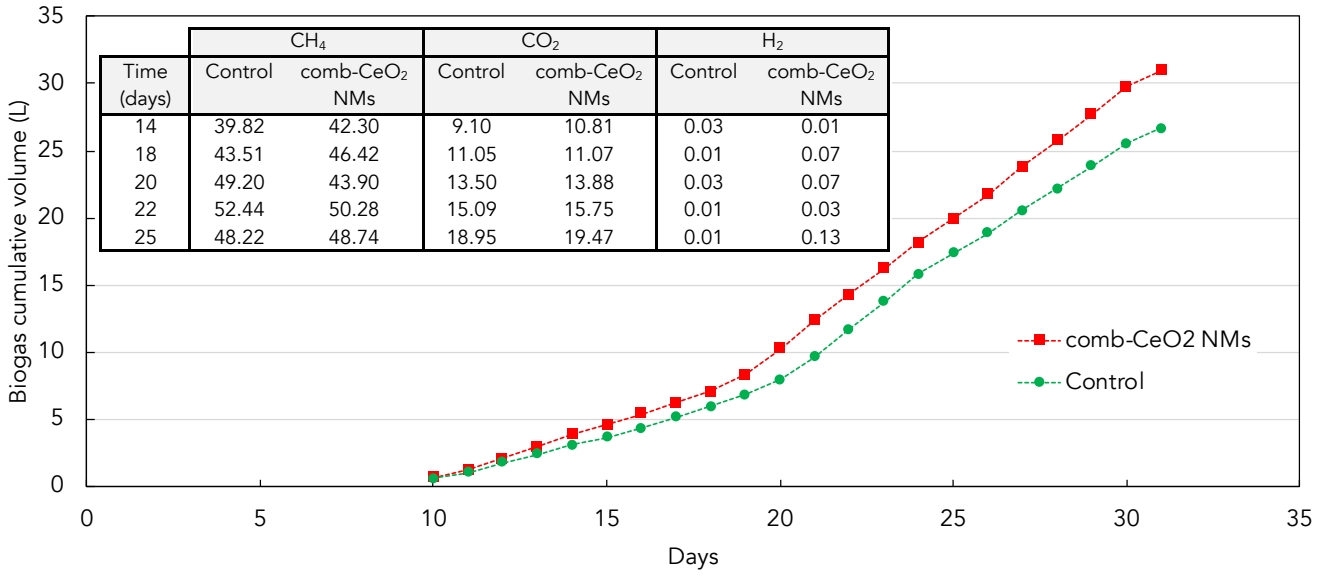

Time (days)	CH_4		CO_2		H_2	
	Control	comb-CeO_2 NMs	Control	comb-CeO_2 NMs	Control	comb-CeO_2 NMs
14	39.82	42.30	9.10	10.81	0.03	0.01
18	43.51	46.42	11.05	11.07	0.01	0.07
20	49.20	43.90	13.50	13.88	0.03	0.07
22	52.44	50.28	15.09	15.75	0.01	0.03
25	48.22	48.74	18.95	19.47	0.01	0.13

Figure 5. Biogas cumulative volume in presence and absence of comb-CeO_2 NMs. Insert: biogas composition in CH_4, CO_2 and H_2 in % vol.

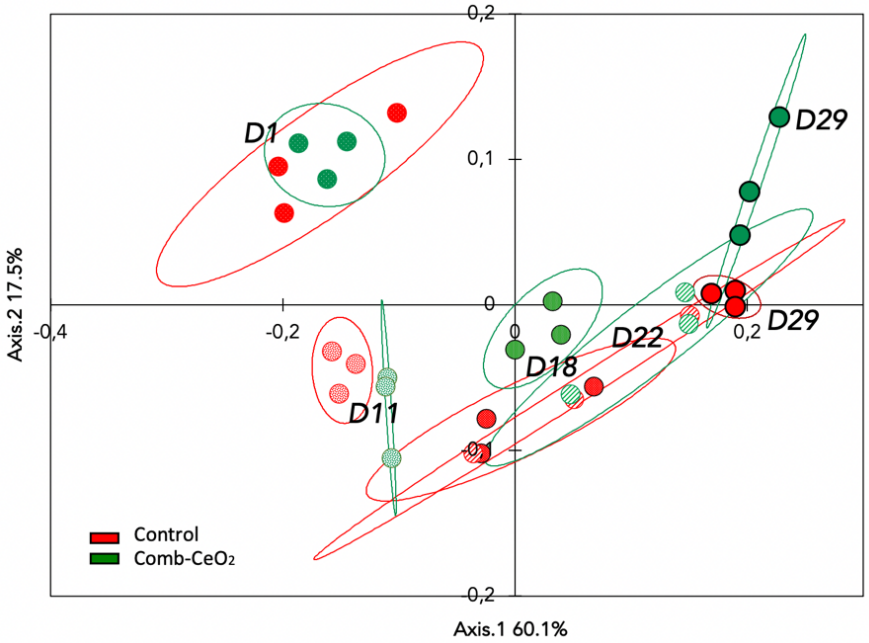

Figure 6. Principal coordinate analysis (PCoA) plot of the weighted UniFrac distance for control AD (red dots) and comb-CeO_2 contaminated AD (green dots) at day (D) 1, 11, 18, 22 and 29. The percent variation explained by each principal coordinate is indicated on the axes.

To identify the Amplicon Sequence Variants (ASVs) that were the most discriminatory overtime between the control and the contaminated AD, a longitudinal feature volatility analysis at the ASV level was performed (Figure 7 and **Erreur ! Source du renvoi introuvable.**). Methanogenesis is exclusively performed by distinct groups of *archaea*. Hydrogenotrophic methanogens produce CH_4 from CO_2 and H_2 or formate. Methylotrophic methanogens can grow on methylated compounds (*e.g.* methanol) and acetoclastic methanogens directly dismutate acetate to CH_4 [67]. Syntrophic acetate oxidizing bacteria can compete with acetoclastic *archaea* by consuming acetate, to produce H_2 and CO_2 or formate that be converted to CH_4 by hydrogenotrophic methanogens [67] while H_2-consuming acetogenic bacteria, compete with hydrogenotrophic methanogens, by converting H_2 to acetate [68].

The two most important ASVs (Important Features IF>0.1) were identified as *Methanosphaerula* genus, within the *Methanomicrobiales* order. *Methanomicrobiales* are strictly CO_2 reducing methanogens, using H_2 or formate as the reducing agent [69]. **Erreur ! Source du renvoi introuvable.** shows that the relative abundances of these hydrogenotrophic methanogens were higher in the comb-CeO_2 AD. The third ASV (IF 0.083) is related to *Clostridium* genus, whose abundance was sporadically higher at Day 11 in control AD (see SI for a dynamic view of IF). *Clostridium* possesses

cellulolytic and H_2-producing activities, both properties are likely essential for an efficient degradation of the biomass [70]. Then a group of four ASVs (0.039<IF<0.08) were affiliated to one *Methanocorpusculum genus*, within hydrogenotrophic order *Methanomicrobiales*, and three *Methanosarcina* genera, within acetoclastic/methylotrophic/hydrogenotrophic *Methanosarcinaceae* family. The relative abundances of these ASVs were temporally identical in both reactors, and showed a drastic increase from Day 18 onwards, which corresponds to the detection of CH_4 in the biogas. Within the next important features, four ASVs related to *Methanosarcina* showed higher relative abundances in control AD after Day 22, while an ASV related to *Kosmotoga* genus within *Thermotogaceae* family was found more abundant in comb-CeO_2 AD. Bacteria in the *Thermotogaceae* family produce thermostable enzymes that degrade complex sugars, with high production rates of H_2 [71]. Hydrogenetrophic and acetoclastic production of methane can coexist in digesters [72]. However, the importance of *Methanomicrobiales* and H_2 related bacteria in the Feature Volatility Analysis suggests that a hydrogenotrophic pathway could be favored in the comb-CeO_2 contaminated AD.

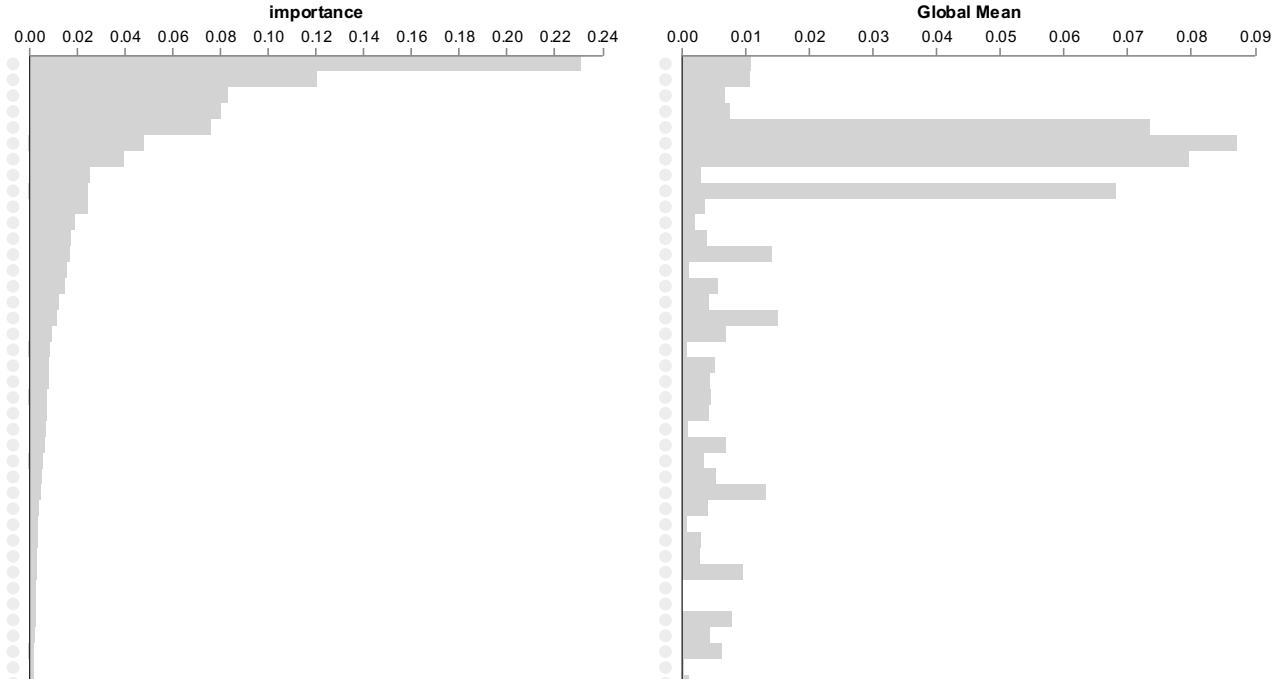

Figure 7. Longitudinal feature volatility analysis at the ASV level: important ASV for the microbiome progression overtime (left). Mean relative abundance for each ASV (right).

To deepen the analysis, a Linear Discriminant Analysis Effect Size (LEfSe) at D29 (Figure 8) was performed. 46 discriminatory taxa (Linear discriminant analysis score >3 or <-3, p<0.05) are summarized in **Erreur ! Source du renvoi introuvable.**. In control AD, hydrogenotrophic *Methanomicrobiales* and acetoclastic *Methanosarcinales* were enriched, together with H_2-consuming acetogenic bacteria (*Treponema* genus and taxa within the *Lachnospiraceae* familiy) [73]. LEfSe highlighted that comb-CeO_2 increased the abundance in: (i) *Bacteroidetes* phyla, associated with high hydrolytic activity [74] which is in line with the high lipase and **α**-glucosidase activities measured in comb-CeO_2 contaminated-AD, (ii) hydrogenotrophic methanogen *archaea* within the *Methanomicrobiale* order (*e.g. Methanoculleus, Methanobacterium*), (iii) syntrophic acetate oxidizing bacteria as *Synergistes* [75] and *Firmicutes* [72,76] phyla. All these changes are indicative of a shift of the methanogenesis through an hydrogenotrophic pathway in presence of comb-CeO_2 during digestion.

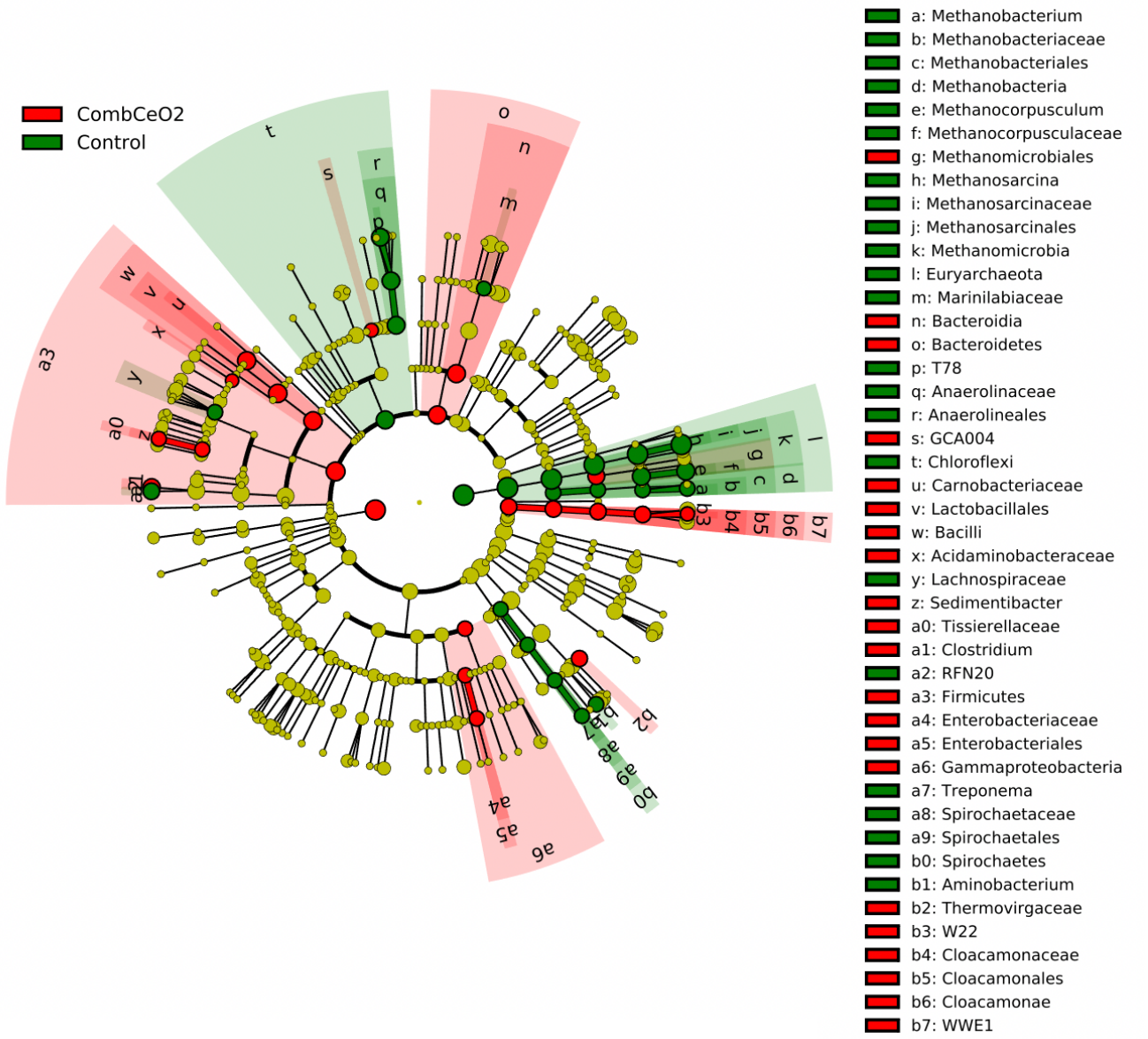

Figure 8. Differentially abundant taxa between the control and contaminated AD**:** Linear Discriminant Analysis Effect Size (LEfSe) cladogram of differentially abundant taxa at D29, in control (green) and comb-CeO_2 contaminated AD (red).

These results are important to understand the synergistic relations between microorganisms and AD performance chronically contaminated with emerging pollutants such as NMs. In the existing literature, a few authors have studied the impacts of high concentrations of pristine CeO_2 NMs on anaerobic treatment and observed different and even contradictory results. García et al. (2012) have shown a great inhibition of biogas production after 50 days of AD in presence of pristine CeO_2 NMs (640 mg L^{-1}, 12 nm diameter) [17]. It is noteworthy that mesophilic and thermophilic anaerobic consortia were drastically inhibited (up to 90%) at these concentrations [17]. In contrast, Ünsar et al. (2016) measured only 5.5 % inhibition in Biochemical Methane Potential assays following exposure to pristine CeO_2 NMs (5 680 mg.L^{-1}, 15-30 nm diameter) [20]. It is difficult to compare these contradictory results with ours because of the drastic difference in CeO_2 concentrations and considering that CeO_2 NMs were combusted in our experimental conditions. From an operational point of view, the increased biogas production and energy recovery was a positive outcome of the presence of 2.2 mg.L^{-1} of comb-CeO_2 NMs, which induced changes in metabolic pathways from acetoclastic to hydrogenotrophic methane production. The cumulative volume of biogas production increased by ~25% after 20 days which corresponds to one solid retention time in our experimental conditions. Such positive effects were also observed in a previous study with pristine TiO_2 NMs that increased methane production by 14.9% [9]. Consequently, while the magnitude of daily methane production was low, it represents a non-negligible cumulative amount over long periods of time.

Conclusion

This study combines expertise in chemical engineering, microbiology and physical chemistry to assess the impacts of the latest stage of the NMs lifecycle on the digestor operation and biogas production in WWTPs. This research used more relevant bioreactor operational settings and contamination scenarios *i.e (i)* operational settings closer to operating conditions used in WWTPs (e.g. SRT between 16 and 20 days for AS and AD, real wastewater from the Aix-en-Provence WWTP, indirect spiking of the AD using contaminated AS, concentrations of NMs near to the environmental predictions) and (*ii*) using aged NMs corresponding to the last stage of their lifecycle. In the context of lifecycle assessment, this study highlights the importance of taking into account the last stages of NMs lifecycle. Pristine and non-aged CeO_2 NMs are often considered as transient NMs via their partial (bio)conversion into Ce(III) in WWTPs [49], during sludge incineration [55], in soils [56], or in plants[57], *i.e.* NMs that transform into other (nanoparticulate) chemical species [53,55]. But considering how these NMs transform during their real-world applications (e.g. combustion in diesel engines), this study shows that CeO_2 NMs may be more persistent than expected even during anaerobic digestion. As such they may be considered conservative NMs in the later stages of their lifecycle (*i.e.* more resistant to transformation in managed waste facilities) due to their enhanced chemical stability acquired during combustion [55].

At the low concentration of aged NMs used during AS production (spiked concentrations of comb-CeO_2-NMs of 130 $\mu g.L^{-1}$), all the physico-chemical and biological proxies showed that comb-CeO_2 NMs neither altered the AS microbial community structure nor the C, P, N removal capacity. However, the presence of 99.9 % of the total CeO_2 injected (without change in speciation) in the AS biosolids altered the production, structure, and activity of the anaerobic sludge during AD (impacting the EPS, ATP, lipase and **α**–glucosidase activities). Interestingly, these modifications to the AS activity shifted the methanogenesis pathways from acetoclastic to hydrogenotrophic and enhanced biogas production with a significant increase in H_2 produced. Indeed, during the whole duration of the experiment, we observed a continuous increase in and non-negligible accumulation of biogas production in the contaminated bioreactor. Herein, we show that combusted CeO_2 NMs could enhance the energy recovery of WWTPs. These findings should be further validated with ever more realistic exposure scenarios, for example by considering mixtures of emerging pollutants in WWTP influent. In the context of the global energy transition, understanding the impacts of emerging pollutants on the efficacy of waste-to-energy conversion in plants is of paramount importance.

Acknowledgements

This work was supported by the French ANR funding for the ANR-3-CESA-0014/NANOSALT program and by the Excellence Initiative of Aix-Marseille University - A*MIDEX, a French "Investissements d'Avenir" program, through its associated Labex SERENADE project. This work is also a contribution to the OSU-Institut Pythéas. The FAME-UHD project is financially supported by the French "grand emprunt" EquipEx (EcoX, ANR-10-EQPX-27-01), the CEA-CNRS CRG consortium and the INSU CNRS institute. Finally, the authors acknowledge the CNRS funding for the IRP iNOVE.

References

1 P. Westerhoff, A. Atkinson, J. Fortner, M. S. Wong, J. Zimmerman, J. Gardea-Torresdey, J. Ranville and P. Herckes, Low risk posed by engineered and incidental nanoparticles in drinking water, *Nat. Nanotechnol.*, 2018, **13**, 661–669.

2 P. Cervantes-Avilés and A. A. Keller, Incidence of metal-based nanoparticles in the conventional wastewater treatment process, *Water Res.*, 2021, **189**, 116603.

3 B. Kim, C.-S. Park, M. Murayama and M. F. Hochella, Discovery and Characterization of Silver Sulfide Nanoparticles in Final Sewage Sludge Products, *Environ. Sci. Technol.*, 2010, **44**, 7509–7514.

4 S. Eduok, C. Hendry, R. Ferguson, B. Martin, R. Villa, B. Jefferson and F. Coulon, Insights into the effect of mixed engineered nanoparticles on activated sludge performance, *FEMS Microbiol. Ecol.*, 2015, **91**, fiv082–fiv082.

5 B. Nowack and T. D. Bucheli, Occurrence, behavior and effects of nanoparticles in the environment, *Env. Pollut*, 2007, **150**, 5–22.

6 T. M. Benn and P. Westerhoff, Nanoparticle silver released into water from commercially available sock fabrics, *Environ. Sci. Technol.*, 2008, **42**, 4133–4139.

7 F. Gottschalk, T. Sun and B. Nowack, Environmental concentrations of engineered nanomaterials: Review of modeling and analytical studies, *Environ. Pollut.*, 2013, **181**, 287–300.

8 A. Lazareva and A. A. Keller, Estimating Potential Life Cycle Releases of Engineered Nanomaterials from Wastewater Treatment Plants, *ACS Sustain. Chem. Eng.*, 2014, **2**, 1656–1665.
9 P. Cervantes-Avilés, J. Ida, T. Toda and G. Cuevas-Rodríguez, Effects and fate of TiO2 nanoparticles in the anaerobic treatment of wastewater and waste sludge, *J. Environ. Manage.*, 2018, **222**, 227–233.
10 F. Gómez-Rivera, J. A. Field, D. Brown and R. Sierra-Alvarez, Fate of cerium dioxide (CeO2) nanoparticles in municipal wastewater during activated sludge treatment, *Bioresour. Technol.*, 2012, **108**, 300–304.
11 L. Barton, M. Therezien, M. Auffan, J.-Y. Bottero and M. Wiesner, Theory and methodology for determining nanoparticle affinity for heteroaggregation in environmental matrices using batch measurements, *Environ. Eng. Sci.*, 2014, **31**, 421–427.
12 E. Lombi, E. Donner, S. Taheri, E. Tavakkoli, Å. K. Jämting, S. McClure, R. Naidu, B. W. Miller, K. G. Scheckel and K. Vasilev, Transformation of four silver/silver chloride nanoparticles during anaerobic treatment of wastewater and post-processing of sewage sludge, *Environ. Pollut.*, 2013, **176**, 193–197.
13 C. Zhang, Z. Liang and Z. Hu, Bacterial response to a continuous long-term exposure of silver nanoparticles at sub-ppm silver concentrations in a membrane bioreactor activated sludge system, *Water Res.*, 2014, **50**, 350–358.
14 H. Chen, Y. Chen, X. Zheng, X. Li and J. Luo, How does the entering of copper nanoparticles into biological wastewater treatment system affect sludge treatment for VFA production, *Water Res*, 2014, **63**, 125–134.
15 B. Demirel, The impacts of engineered nanomaterials (ENMs) on anaerobic digestion processes, *Process Biochem*, 2016, **51**, 308–313.
16 D. Wang and Y. Chen, Critical review of the influences of nanoparticles on biological wastewater treatment and sludge digestion, *Crit. Rev. Biotechnol.*, 2016, **36**, 816–828.
17 A. García, L. Delgado, J. A. Torà, E. Casals, E. González, V. Puntes, X. Font, J. Carrera and A. Sánchez, Effect of cerium dioxide, titanium dioxide, silver, and gold nanoparticles on the activity of microbial communities intended in wastewater treatment, *J Hazard Mater*, 2012, **199**, 64–72.
18 J. Ma, X. Quan, X. Si and Y. Wu, Responses of anaerobic granule and flocculent sludge to ceria nanoparticles and toxic mechanisms, *Bioresour Technol*, 2013, **149**, 346–352.
19 A. Gogos, J. Wielinski, A. Voegelin, H. Emerich and R. Kaegi, Transformation of cerium dioxide nanoparticles during sewage sludge incineration, *Environ. Sci. Nano*, 2019, **6**, 1765–1776.
20 E. K. Ünşar, A. S. Çığgın, A. Erdem and N. A. Perendeci, Long and short-term impacts of CuO, Ag and CeO2 nanoparticles on anaerobic digestion of municipal waste activated sludge, *Env. Sci Process Impacts*, 2016, **18**, 277–288.
21 S. Eduok, R. Ferguson, B. Jefferson, R. Villa and F. Coulon, Aged-engineered nanoparticles effect on sludge anaerobic digestion performance and associated microbial communities, *Sci. Total Environ.*, 2017, **609**, 232–241.
22 M. Auffan, W. Liu, L. Brousset, L. Scifo, A. Pariat, M. Sanles, P. Chaurand, B. Angeletti, A. Thiery, A. Masion and J. Rose, Environmental exposure of a simulated pond ecosystem to CuO nanoparticle based-wood stain throughout its life cycle, *Environ. Sci. Nano*, 2018, **5**, 2579–2589.
23 L. Scifo, P. Chaurand, N. Bossa, A. Avelan, M. Auffan, A. Masion, B. Angeletti, I. Kieffer, J. Labille, J.-Y. Bottero and J. Rose, Non-linear release dynamics for a CeO2 nanomaterial embedded in a protective wood stain, due to matrix photo-degradation, *Environ. Pollut.*
24 G. Wakefield, X. Wu, M. Gardener, B. Park and S. Anderson, Envirox™ fuel-borne catalyst: Developing and launching a nano-fuel additive, *Technol. Anal. Strateg. Manag.*, 2008, **20**, 127–136.
25 B. Park, K. Donaldson, R. Duffin, L. Tran, F. Kelly, I. Mudway, J.-P. Morin, R. Guest, P. Jenkinson, Z. Samaras, M. Giannouli, H. Kouridis and P. Martin, Hazard and Risk Assessment of a Nanoparticulate Cerium Oxide-Based Diesel Fuel Additive, a Case Study, *Inhal. Toxicol.*, 2008, **20**, 547–566.
26 B. J. Majestic, G. B. Erdakos, M. Lewandowski, K. D. Oliver, R. D. Willis, T. E. Kleindienst and P. V. Bhave, A review of selected engineered nanoparticles in the atmosphere, sources, transformations, and techniques for sampling and analysis, *Int J Occup Env. Health*, 2010, **16**, 488–507.

27 A. Johnson and B. Park, Predicting contamination by the fuel additive cerium oxide engineered nanoparticles within the United Kingdom and the associated risks, *Environ. Toxicol. Chem.*, 2012, **31**, 2582–2587.
28 B. Gantt, S. Hoque, R. D. Willis, K. M. Fahey, J. M. Delgado-Saborit, R. M. Harrison, G. B. Erdakos, P. V. Bhave, K. M. Zhang, K. Kovalcik and H. O. T. Pye, Near-Road Modeling and Measurement of Cerium-Containing Particles Generated by Nanoparticle Diesel Fuel Additive Use, *Environ. Sci. Technol.*, 2014, **48**, 10607–10613.
29 J. G. Dale, S. S. Cox, M. E. Vance, L. C. Marr and M. F. Hochella, Transformation of Cerium Oxide Nanoparticles from a Diesel Fuel Additive during Combustion in a Diesel Engine, *Environ. Sci. Technol.*, 2017, **51**, 1973–1980.
30 B. Giese, F. Klaessig, B. Park, R. Kaegi, M. Steinfeldt, H. Wigger, A. von Gleich and F. Gottschalk, Risks, release and concentrations of engineered nanomaterial in the environment, *Sci. Rep.*, 2018, **8**, 1–18.
31 K. Phalyvong, Y. Sivry, H. Pauwels, A. Gélabert, M. Tharaud, G. Wille, X. Bourrat, J. F. Ranville and M. F. Benedetti, Assessing CeO2 and TiO2 nanoparticle concentrations in the Seine River and its tributaries near Paris, *Front. Environ. Sci.*, 2021, 271.
32 G. E. Batley, B. Halliburton, J. K. Kirby, C. L. Doolette, D. Navarro, M. J. McLaughlin and C. Veitch, Characterization and ecological risk assessment of nanoparticulate CeO2 as a diesel fuel catalyst, *Environ. Toxicol. Chem.*, 2013, **32**, 1896–1905.
33 M. Auffan, M. Tella, W. Liu, A. Pariat, M. Cabie, D. Borschneck, B. Angeletti, G. Landrot, C. Mouneyrac, L. Giamberini and J. Rose, Structural and physical-chemical behavior of a CeO2 nanoparticle based diesel additive during combustion and environmental release, *Environ. Sci. Nano*, 2017, **4**, 1974–1980.
34 M. Cotena, M. Auffan, S. Robert, V. Tassistro, N. Resseguier, J. Rose and J. Perrin, CeO2 Nanomaterials from Diesel Engine Exhaust Induce DNA Damage and Oxidative Stress in Human and Rat Sperm In Vitro, *Nanomaterials*.
35 M. Cotena, M. Auffan, V. Tassistro, N. Resseguier, J. Rose and J. Perrin, In Vitro Co-Exposure to CeO2 Nanomaterials from Diesel Engine Exhaust and Benzo(a)Pyrene Induces Additive DNA Damage in Sperm and Cumulus Cells but Not in Oocytes, *Nanomaterials*, 2021, **11**, 478.
36 J. Zhang, Y. Nazarenko, L. Zhang, L. Calderon, K.-B. Lee, E. Garfunkel, S. Schwander, T. D. Tetley, K. F. Chung, A. E. Porter, M. Ryan, H. Kipen, P. J. Lioy and G. Mainelis, Impacts of a Nanosized Ceria Additive on Diesel Engine Emissions of Particulate and Gaseous Pollutants, *Environ. Sci. Technol.*, 2013, **47**, 13077–13085.
37 L. S. Clesceri, A. E. Greenberg and A. D. Eaton, *Standard Methods for the Examination of Water and Wastewater*, American Public Health Association., 1998, vol. 20th ed.
38 R. Goel, T. Mino, H. Satoh and T. Matsuo, Enzyme activities under anaerobic and aerobic conditions in activated sludge sequencing batch reactor, *Water Res.*, 1998, **32**, 2081–2088.
39 H.-W. Kim, J.-Y. Nam, S.-T. Kang, D.-H. Kim, K.-W. Jung and H.-S. Shin, Hydrolytic activities of extracellular enzymes in thermophilic and mesophilic anaerobic sequencing-batch reactors treating organic fractions of municipal solid wastes, *Bioresour Technol*, 2012, **110**, 130–134.
40 S. Akkache, I. Seyssiecq and N. Roche, Effect of exo-polysaccharide concentration in the rheological properties and settling ability of activated sludge, *Env. Technol*, 2013, **34**, 2995–3003.
41 O. Proux, E. Lahera, W. Del Net, I. Kieffer, M. Rovezzi, D. Testemale, M. Irar, S. Thomas, A. Aguilar-Tapia, E. F. Bazarkina, A. Prat, M. Tella, M. Auffan, J. Rose and J.-L. Hazemann, High-Energy Resolution Fluorescence Detected X-Ray Absorption Spectroscopy: A Powerful New Structural Tool in Environmental Biogeochemistry Sciences, *J. Environ. Qual.*, 2017, **46**, 1146–1157.
42 B. Ravel and M. Newville, ATHENA, ARTEMIS, HEPHAESTUS: data analysis for X-ray absorption spectroscopy using IFEFFIT, *J Synchrotron Radiat*, 2005, **12**, 537–541.
43 A. E. Parada, D. M. Needham and J. A. Fuhrman, Every base matters: assessing small subunit rRNA primers for marine microbiomes with mock communities, time series and global field samples, *Environ. Microbiol.*, 2016, **18**, 1403–1414.

44 A. Apprill, S. McNally, R. Parsons and L. Weber, Minor revision to V4 region SSU rRNA 806R gene primer greatly increases detection of SAR11 bacterioplankton, *Aquat. Microb. Ecol.*, 2015, **75**, 129–137.
45 E. Bolyen, J. R. Rideout, M. R. Dillon, N. A. Bokulich, C. C. Abnet, G. A. Al-Ghalith, H. Alexander, E. J. Alm, M. Arumugam, F. Asnicar, Y. Bai, J. E. Bisanz, K. Bittinger, A. Brejnrod, C. J. Brislawn, C. T. Brown, B. J. Callahan, A. M. Caraballo-Rodríguez, J. Chase, E. K. Cope, R. Da Silva, C. Diener, P. C. Dorrestein, G. M. Douglas, D. M. Durall, C. Duvallet, C. F. Edwardson, M. Ernst, M. Estaki, J. Fouquier, J. M. Gauglitz, S. M. Gibbons, D. L. Gibson, A. Gonzalez, K. Gorlick, J. Guo, B. Hillmann, S. Holmes, H. Holste, C. Huttenhower, G. A. Huttley, S. Janssen, A. K. Jarmusch, L. Jiang, B. D. Kaehler, K. B. Kang, C. R. Keefe, P. Keim, S. T. Kelley, D. Knights, I. Koester, T. Kosciolek, J. Kreps, M. G. I. Langille, J. Lee, R. Ley, Y.-X. Liu, E. Loftfield, C. Lozupone, M. Maher, C. Marotz, B. D. Martin, D. McDonald, L. J. McIver, A. V. Melnik, J. L. Metcalf, S. C. Morgan, J. T. Morton, A. T. Naimey, J. A. Navas-Molina, L. F. Nothias, S. B. Orchanian, T. Pearson, S. L. Peoples, D. Petras, M. L. Preuss, E. Pruesse, L. B. Rasmussen, A. Rivers, M. S. Robeson, P. Rosenthal, N. Segata, M. Shaffer, A. Shiffer, R. Sinha, S. J. Song, J. R. Spear, A. D. Swafford, L. R. Thompson, P. J. Torres, P. Trinh, A. Tripathi, P. J. Turnbaugh, S. Ul-Hasan, J. J. J. van der Hooft, F. Vargas, Y. Vázquez-Baeza, E. Vogtmann, M. von Hippel, W. Walters, Y. Wan, M. Wang, J. Warren, K. C. Weber, C. H. D. Williamson, A. D. Willis, Z. Z. Xu, J. R. Zaneveld, Y. Zhang, Q. Zhu, R. Knight and J. G. Caporaso, Reproducible, interactive, scalable and extensible microbiome data science using QIIME 2, *Nat. Biotechnol.*, 2019, **37**, 852–857.
46 B. J. Callahan, P. J. McMurdie, M. J. Rosen, A. W. Han, A. J. A. Johnson and S. P. Holmes, DADA2: High-resolution sample inference from Illumina amplicon data, *Nat. Methods*, 2016, **13**, 581–583.
47 K. Katoh and D. M. Standley, MAFFT Multiple Sequence Alignment Software Version 7: Improvements in Performance and Usability, *Mol. Biol. Evol.*, 2013, **30**, 772–780.
48 M. N. Price, P. S. Dehal and A. P. Arkin, FastTree: Computing Large Minimum Evolution Trees with Profiles instead of a Distance Matrix, *Mol. Biol. Evol.*, 2009, **26**, 1641–1650.
49 N. A. Bokulich, M. R. Dillon, Y. Zhang, J. R. Rideout, E. Bolyen, H. Li, P. S. Albert and J. G. Caporaso, q2-longitudinal: longitudinal and paired-sample analyses of microbiome data, *MSystems*, 2018, **3**, e00219-18.
50 L. K. Limbach, R. Bereiter, E. Müller, R. Krebs, R. Gälli and W. J. Stark, Removal of Oxide Nanoparticles in a Model Wastewater Treatment Plant: Influence of Agglomeration and Surfactants on Clearing Efficiency, *Environ. Sci. Technol.*, 2008, **42**, 5828–5833.
51 M. A. Kiser, P. Westerhoff, T. Benn, Y. Wang, J. Pérez-Rivera and K. Hristovski, Titanium Nanomaterial Removal and Release from Wastewater Treatment Plants, *Environ. Sci. Technol.*, 2009, **43**, 6757–6763.
52 R. Kaegi, A. Voegelin, B. Sinnet, S. Zuleeg, H. Hagendorfer, M. Burkhardt and H. Siegrist, Behavior of Metallic Silver Nanoparticles in a Pilot Wastewater Treatment Plant, *Environ. Sci. Technol.*, 2011, **45**, 3902–3908.
53 L. Barton, M. Auffan, M. Bertrand, M. Barakat, C. Santaella, A. Masion, D. Borschneck, L. Olivi, N. Roche, M. Wiesner and J.-Y. Bottero, Transformation of pristine and citrate-functionalized CeO2 nanoparticles in a laboratory-scale activated sludge reactor, *Environ. Sci. Technol.*, 2014, **48**, 7289–7296.
54 J.-D. Cafun, K. O. Kvashnina, E. Casals, V. F. Puntes and P. Glatzel, Absence of Ce3+ Sites in Chemically Active Colloidal Ceria Nanoparticles, *ACS Nano*, 2013, **7**, 10726–10732.
55 J. Wielinski, A. Gogos, A. Voegelin, C. R. Müller, E. Morgenroth and R. Kaegi, Release of gold (Au), silver (Ag) and cerium dioxide (CeO 2) nanoparticles from sewage sludge incineration ash, *Environ. Sci. Nano*, 2021, **8**, 3220–3232.
56 C. Jiao, C. Dong, W. Dai, W. Luo, S. Fan, L. Zhou, Y. Ma, X. He and Z. Zhang, Geochemical cycle of exogenetic CeO2 nanoparticles in agricultural soil: Chemical transformation and re-distribution, *Nano Today*, 2022, **46**, 101563.
57 P. Zhang, Z. Guo, F. A. Monikh, I. Lynch, E. Valsami-Jones and Z. Zhang, Growing rice (Oryza sativa) aerobically reduces phytotoxicity, uptake, and transformation of CeO2 nanoparticles, *Environ. Sci. Technol.*, 2021, **55**, 8654–8664.

58 I. T. Jolliffe and J. Cadima, Principal component analysis: a review and recent developments, *Philos. Trans. R. Soc. Math. Phys. Eng. Sci.*, 2016, **374**, 20150202.
59 G. You, J. Hou, Y. Xu, C. Wang, P. Wang, L. Miao, Y. Ao, Y. Li and B. Lv, Effects of CeO2 nanoparticles on production and physicochemical characteristics of extracellular polymeric substances in biofilms in sequencing batch biofilm reactor, *Bioresour Technol*, 2015, **194**, 91–98.
60 G.-P. Sheng, H.-Q. Yu and X.-Y. Li, Extracellular polymeric substances (EPS) of microbial aggregates in biological wastewater treatment systems: A review, *Biotechnol Adv*, 2010, **28**, 882–894.
61 Q. Feng, Y. Sun, Y. Wu, Z. Xue, J. Luo, F. Fang, C. Li and J. Cao, Physicochemical and Biological Effects on Activated Sludge Performance and Activity Recovery of Damaged Sludge by Exposure to CeO2 Nanoparticles in Sequencing Batch Reactors, *Int. J. Environ. Res. Public. Health*, 2019, **16**, 4029.
62 J. Song, Y. Xu, C. Liu, Q. He, R. Huang, S. Jiang, J. Ma, Z. Wu and X. Huangfu, Interpreting the role of NO3−, SO42−, and extracellular polymeric substances on aggregation kinetics of CeO2 nanoparticles: Measurement and modeling, *Ecotoxicol. Environ. Saf.*, 2020, **194**, 110456.
63 M. Auffan, A. Masion, J. Labille, M. A. Diot, W. Liu, L. Olivi, O. Proux, F. Ziarelli, P. Chaurand, C. Geantet, J.-Y. Bottero and J. Rose, Long-term aging of a CeO2 based nanocomposite used for wood protection, *Environ. Pollut.*, 2014, **188**, 1–7.
64 H. Mu and Y. Chen, Long-term effect of ZnO nanoparticles on waste activated sludge anaerobic digestion, *Water Res.*, 2011, **45**, 5612–5620.
65 C. Mao, Y. Feng, X. Wang and G. Ren, Review on research achievements of biogas from anaerobic digestion, *Renew. Sustain. Energy Rev.*, 2015, **45**, 540–555.
66 P. Ghosh, M. Kumar, R. Kapoor, S. S. Kumar, L. Singh, V. Vijay, V. K. Vijay, V. Kumar and I. S. Thakur, Enhanced biogas production from municipal solid waste via co-digestion with sewage sludge and metabolic pathway analysis, *Bioresour. Technol.*, 2020, **296**, 122275.
67 B. Wintsche, N. Jehmlich, D. Popp, H. Harms and S. Kleinsteuber, Metabolic adaptation of methanogens in anaerobic digesters upon trace element limitation, *Front. Microbiol.*, 2018, **9**, 405.
68 S. Karekar, R. Stefanini and B. Ahring, Homo-Acetogens: Their Metabolism and Competitive Relationship with Hydrogenotrophic Methanogens, *Microorganisms*, 2022, **10**, 397.
69 Y. Liu, *Methanobacteriales*, 2010.
70 R. Wirth, G. Lakatos, T. Böjti, G. Maróti, Z. Bagi, M. Kis, A. Kovács, N. Ács, G. Rákhely and K. L. Kovács, Metagenome changes in the mesophilic biogas-producing community during fermentation of the green alga Scenedesmus obliquus, *J. Biotechnol.*, 2015, **215**, 52–61.
71 N. Esercizio, M. Lanzilli, M. Vastano, S. Landi, Z. Xu, C. Gallo, G. Nuzzo, E. Manzo, A. Fontana and G. d'Ippolito, Fermentation of Biodegradable Organic Waste by the Family Thermotogaceae, *Resources*, 2021, **10**, 34.
72 S. Dyksma, L. Jansen and C. Gallert, Syntrophic acetate oxidation replaces acetoclastic methanogenesis during thermophilic digestion of biowaste, *Microbiome*, 2020, **8**, 1–14.
73 L. Li, Q. He, Y. Ma, X. Wang and X. Peng, A mesophilic anaerobic digester for treating food waste: process stability and microbial community analysis using pyrosequencing, *Microb. Cell Factories*, 2016, **15**, 1–11.
74 M. A. Khan, S. T. Khan, M. C. Sequeira, S. M. Faheem and N. Rais, Illumina sequencing of 16S rRNA genes reveals a unique microbial community in three anaerobic sludge digesters of Dubai, *PloS One*, 2021, **16**, e0249023.
75 K. Nakasaki, M. Koyama, T. Maekawa and J. Fujita, Changes in the microbial community during the acclimation process of anaerobic digestion for treatment of synthetic lipid-rich wastewater, *J. Biotechnol.*, 2019, **306**, 32–37.
76 J. W. Lim, T. Park, Y. W. Tong and Z. Yu, in *Advances in Bioenergy*, Elsevier, 2020, vol. 5, pp. 1–61.